Role of microscopic temperature-dependent binding energies in the decay of ^{32}Si* formed in the ^{20}O + ^{12}C reaction

Manpreet Kaur [1,2,*] BirBikram Singh [3,4,†] and S. K. Patra [1,2]

[1]*Institute of Physics, Sachivalaya Marg, Bhubaneswar-751005, India*
[2]*Homi Bhabha National Institute, Anushakti Nagar, Mumbai-400094, India*
[3]*Department of Physics, Sri Guru Granth Sahib World University, Fatehgarh Sahib-140406, India*
[4]*Department of Physics, Akal University, Talwandi Sabo-151302, India*

The investigation of fusion reactions involving light neutron-rich exotic nuclei is of paramount significance to understand nucleosynthesis in astrophysical scenarios. It is also estimated as a possible heat source to ignite ^{12}C + ^{12}C reaction and production of x-ray superbursts from accreting neutron star. Recently, the fusion of neutron-rich ^{20}O with ^{12}C target has been studied with measurement of fusion cross-section (σ_{fus}). Bass model under predicts the σ_{fus} and time-dependent Hartree-Fock model also fails to explain the experimental data. To explicate the same, the investigation of ^{20}O + ^{12}C reaction at near barrier energies has been made within quantum mechanical fragmentation-based dynamical cluster-decay model (DCM). Within DCM, the fragmentation potential comprises temperature-dependent Coulomb, nuclear and centrifugal potentials, along with temperature-dependent binding energies (T.B.E.) calculated within the macroscopic approach of Davidson mass formula. Recently, we have explored the temperature-dependence of different nuclear properties and nuclear symmetry energy within microscopic relativistic mean-field (RMF) theory [M. Kaur *et al.*, Nucl. Phys. A **1000**, 121871 (2020)]. In the present work, we inculcate the microscopic T.B.E. from RMF theory within DCM and investigate the structure of fragmentation potential for ^{32}Si* formed in ^{20}O + ^{12}C reaction, comparatively for macroscopic (mac) and microscopic (mic) T.B.E. obtained from Davidson mass formula and RMF theory, respectively. The structure and magnitude of fragmentation potential are found to change drastically/notably along with a change in energetically favored/minimized fragments for both choices of T.B.E. The α particles (^{4}He, ^{5}He) are favored at lower angular momenta in fragmentation profile for mic T.B.E. case only, which is in the agreement with predictions of statistical model results. This change in the nuclear structure embodied via fragmentation potential energy carries its imprints in the preformation probability P_0 of different fragments and affects the contribution of individual light-charged particle (LCP) channel in the σ_{fus}. A comparison of the relative cross-section of different LCP channels toward σ_{fus} is quite different for both cases of T.B.E. The cross-section of ^{2}H and ^{4}He LCP channels is relatively enhanced for mic T.B.E. compared to mac T.B.E. Among different LCP channels, the ^{5}He channel is the major contributor in σ_{fus}, which is in line with the results of the statistical EVAPOR model. The DCM-calculated σ_{fus} is in agreement with the experimental data.

I. INTRODUCTION

The heavy-ion-induced fusion reactions with both stable and unstable nuclei have captured the central attention both experimentally and theoretically. Besides the production of exotic nuclei toward the drip lines, the extension of periodic table up to superheavy elements, and energy production, these studies are crucial to unfold the origin of elements via nucleosynthesis in the celestial laboratory [1–7]. The fusion reactions of carbon and oxygen nuclei at near-barrier energies are of immense importance in astrophysical scenarios. The outer crust of an accreting neutron star offers a peculiar environment for the occurrence of nuclear reactions. The fusion reactions involving neutron-rich light nuclei are anticipated

as a viable heat source to stimulate ^{12}C + ^{12}C reaction and production of x-ray superburst [6]. The radioactive ion beam facilities open up the window to explore such possibilities.

Some studies have reported that fusion probability for neutron-rich heavy beams is enhanced compared to β-stable beams at below and near-barrier energies [2,3,7,8]. It has been linked with the increased significance of neutron transfer channels leading to effective lowering of the Coulomb barrier. However, very limited data is available experimentally and/or theoretically for fusion reactions involving light neutron-rich nuclei. The fusion cross-section for ^{20}O + ^{12}C has been measured experimentally by Rudolph *et al.* [9], which shows an enhancement compared to Bass model [10] predictions. Also, the time-dependent Hartree Fock (TDHF) model was applied to this reaction but could not explain the experimental data. Therefore, it is intriguing to explore the dynamics of such nuclear systems formed in neutron-rich projectile-induced

*manpreetphys@gmail.com
†bir_phy@auts.ac.in

reactions and to compare the fusion cross-section with the experimental data.

Some theoretical approaches such as coupled channel model, semiclassical transport theory, TDHF model, etc. have been employed to study the fusion enhancement in sub and near-barrier domain [11–13]. Dynamical cluster-decay model (DCM) [14–17], based upon quantum mechanical fragmentation theory (QMFT), has also been applied successfully to explore the decay of hot nuclear systems formed in reactions induced by stable and unstable projectiles. Within DCM, the temperature evolution of clustering effects in light mass α and non-α conjugate systems and its subsequent effect on the decay yield has been probed [15]. The dynamics of neutron-rich light and mid mass compound systems have also been explored within DCM [18–20]. To study the excited state decay, all the potentials within DCM are temperature-dependent and the knowledge of temperature-dependent binding energies is crucial. The binding energy of a nucleus at T temperature, one of the fundamental ingredients of the DCM, is defined as the sum of liquid drop energy $V_{\text{LDM}}(T)$ and shell correction within the Strutinsky renormalization procedure [21]. So far, the temperature-dependent liquid drop model binding energies of Davidson formula [22] together with the shell corrections by Myers-Swiatecki [23] have been used within DCM. It is important to point out that the masses of known regimes at $T = 0$ MeV have been employed in the fitting of different mass formulas and an obvious agreement with experimental data is anticipated in these regions. However, the point of concern is their divergence in the unknown regions where no common trend or correlation is seen (see Fig. 4 of Ref. [24]) taking one of the mass formula as a reference case [25,26]. This divergence cast doubt upon the predictive efficacy of different mass models. Therefore, any available mass formula cannot be used as a reliable guide to get temperature-dependent binding energies.

Here, we address this issue by the inculcation of temperature-dependent binding energies from the microscopic relativistic mean-field (RMF) theory [27,28] within DCM. Since it is well known that any theory expressed in the form of differential equations, e.g., Schrödinger, Dirac equation, etc., has intrinsic predictive power. Within RMF theory, the interaction among nucleons is assumed to occur via the exchange of isoscalar-scalar σ, isovector-vector ρ, and isoscalar-vector ω mesons. Another, distinct advantage of RMF theory is that it automatically takes account of spin-orbit interaction, i.e., additional inclusion of shell corrections in the binding energies is not required. The Dirac equation and Klein-Gordon equations for nucleons and mesons, respectively, are solved self-consistently which give different nuclear properties. Here, nuclear properties such as binding energies, radius, etc. of only a few doubly magic nuclei are fitted at $T = 0$ MeV with reference to experimental data and predictions made for other thousands of nuclei are in consonance with experimental data at $T = 0$ MeV. Therefore, the prediction of temperature-dependent binding energies by RMF theory is reliable. In recent work, two of us (MK and SKP) have studied the temperature-dependence of different bulk properties of rare earth nuclei within RMF theory and also investigated the temperature-dependence of symmetry energy and its volume

and surface components using temperature-dependent RMF densities [28].

In the view of the above discussions, it is interesting to investigate the reaction involving light exotic nuclei, which is of astrophysical significance. Also, it is quite important to explore the role of microscopic temperature-dependent binding energies [27–29] upon the fragmentation process and different variables involved in the fusion cross-section estimation of low energy reactions. In the present work, we aim to probe the dynamics of $^{32}\text{Si}^*$ nuclear system formed in $^{20}\text{O} + ^{12}\text{C}$ reaction at near-barrier energies [9] together with the influence of microscopic T-dependent binding energies upon the contribution of different emission channels in fusion cross-section within DCM. The theoretical frameworks of RMF theory and DCM are discussed in Sec. II, and results are discussed in Sec. III. The summary of the work is presented in Sec. IV.

II. THEORETICAL FORMALISMS

A. Relativistic mean-field (RMF) theory

RMF theory is one of the microscopic approaches to solve many-body problems of the nuclear system. Within RMF model, the nucleons are assumed to interact through the exchange of mesons. For the sake of completeness, here we present the RMF formalism briefly. The details of the RMF model can be found in Refs. [30,31]. The Lagrangian density of nucleons with σ, ω, ρ mesons and photon A^μ fields within RMF is given as

$$
\begin{aligned}
\mathcal{L} = {} & \bar{\psi}(i\gamma^\mu \partial_\mu - M)\psi + \tfrac{1}{2}\big(\partial^\mu \sigma \partial_\mu \sigma - m_s^2 \sigma^2\big) \\
& - \tfrac{1}{3}g_2 \sigma^3 - \tfrac{1}{4}g_3 \sigma^4 - g_s \bar{\psi}\psi\sigma \\
& - \tfrac{1}{4}V^{\mu\upsilon}V_{\mu\upsilon} + \tfrac{1}{2}m_\omega^2 \omega^\mu \omega_\mu - g_\omega \bar{\psi}\gamma^\mu \psi \omega_\mu \\
& - \tfrac{1}{4}\vec{R}^{\mu\upsilon}\vec{R}_{\mu\upsilon} + \tfrac{1}{2}m_\rho^2 \vec{\rho}^\mu \vec{\rho}_\mu - g_\rho \bar{\psi}\gamma^\mu \vec{\tau}\psi \vec{\rho_\mu} \\
& - \tfrac{1}{4}F^{\mu\upsilon}F_{\mu\upsilon} - e\bar{\psi}\gamma^\mu \tfrac{(1-\tau_3)}{2}\psi A_\mu,
\end{aligned}
\tag{1}
$$

with

$$V^{\mu\upsilon} = \partial^\mu \omega^\upsilon - \partial^\upsilon \omega^\mu, \tag{2}$$

$$\vec{R}^{\mu\upsilon} = \partial^\mu \vec{\rho}^\upsilon - \partial^\upsilon \vec{\rho}^\mu, \tag{3}$$

$$F^{\mu\upsilon} = \partial^\mu A^\upsilon - \partial^\upsilon A^\mu, \tag{4}$$

where $V_{\mu\nu}$, $\vec{R}_{\mu\nu}$, and $F_{\mu\nu}$ are the antisymmetric tensors corresponding to the vector fields ω_μ, $\vec{\rho}_\mu$, and A^μ, respectively. m_σ, m_ω, and m_ρ are the masses and g_σ, g_ω, g_ρ, $\frac{e^2}{4\pi}$ are the coupling constants for σ, ω, ρ, and photon, respectively. The equations of motion for the baryons and mesons (σ, ω, and ρ) are obtained by solving Lagrangian density using the variational principle and applying the mean-field approximations. These sets of coupled differential equations are solved self-consistently by expanding the Boson and Fermion fields in an axially deformed harmonic oscillator basis with β_0 as the initial deformation. After getting a convergent solution of the fields, the densities and energy of a nucleus are obtained. The total energy of a nucleus at finite temperature T is given by

the expression [27–29,32,33]

$$E(T) = \sum_i \varepsilon_i n_i + E_{\text{mes}} + E_C + E_{\text{pair}} + E_{\text{c.m.}} - AM, \quad (5)$$

where ε_i is the single particle energy, n_i is the occupation probability and E_{mes}, E_C are the contributions of the mesons and Coulomb field. $E_{\text{c.m.}} = -\frac{3}{4} \times 41 A^{-1/3}$ MeV, is the center of mass energy correction obtained from the non-relativistic approximation [34]. E_{pair} is the pairing energy obtained from the BCS formalism [27–29]

$$E_{\text{pair}} = -\triangle \sum_{i>0} u_i v_i = -\frac{\triangle^2}{G}, \quad (6)$$

where u_i^2 and v_i^2 are the probabilities of unoccupied and occupied states, respectively, and $\triangle$ is the pairing gap [35]. The variational approach with respect to the occupation number n_i^2 gives the BCS equation [36,37]:

$$2\epsilon_i u_i v_i - \Delta(u_i^2 - v_i^2) = 0, \quad (7)$$

with the pairing gap $\Delta = G \sum_{i>0} u_i v_i$. The temperature comes into the picture through the occupation number n_i in the formalism given as [27–29]

$$n_i = v_i^2 = \frac{1}{2}\left[1 - \frac{\epsilon_i - \lambda}{\tilde{\epsilon}_i}[1 - 2f(\tilde{\epsilon}_i, T)]\right], \quad (8)$$

where

$$f(\tilde{\epsilon}_i, T) = \frac{1}{(1 + exp[\tilde{\epsilon}_i/T])}$$

is the Fermi Dirac distribution for the quasi particle energy $\tilde{\epsilon}_i$ and $\tilde{\epsilon}_i = \sqrt{(\epsilon_i - \lambda)^2 + \triangle^2}$, where is λ the chemical potential. It is noted that the pairing is important for the binding energy of relatively heavy nuclei but not for light nuclei at $T = 0$ [36]. The present work at finite temperature also involves a negligible contribution of pairing energy in the total binding energy.

The total binding energy $E(T)$ is obtained by subtracting the rest mass energy (AM) of the nucleus, where A is the mass number and M is the nucleonic mass. Then we have used these temperature-dependent binding energies for further calculations of fragmentation potential and preformation probability of different fragments within the dynamical cluster-decay model, discussed in the following subsection.

B. Dynamical cluster-decay model (DCM)

The theoretical approach of DCM [14–17] is discussed briefly here. It is founded upon the quantum mechanical fragmentation theory [38–40], which gives the unified description of binary channels in fusion as well as the fission process. The collective coordinates of the DCM are mass asymmetry $\eta = (A_1 - A_2)/(A_1 + A_2)$ and the relative separation R between centres of two fragments. In terms of above defined collective coordinates, the decay or fragment production cross-section of the compound nucleus (CN), in terms of ℓ partial waves, is [14–17]

$$\sigma = \frac{\pi}{k^2} \sum_{\ell=0}^{\ell_{\text{max}}} (2\ell + 1)P_0 P; \quad k = \sqrt{\frac{2\mu E_{\text{c.m.}}}{\hbar^2}}, \quad (9)$$

where P_0 is the preformation probability, refers to η motion, which gives significant information related to nuclear structure, and P is the penetrability refers to R motion and ℓ_{max} is the maximum angular momentum for which $\sigma_{\text{LP}} \rightarrow 0$. The preformation probability is given as

$$P_0(A_i) = |\psi(\eta(A_i))|^2 \frac{2}{A_{\text{CN}}} \sqrt{B_{\eta\eta}}, \quad (10)$$

where $i = 1, 2$, and $B_{\eta\eta}$ denotes the hydrodynamical mass parameter of Kröger and Scheid [41] based on the hydrodynamical flow. It gives a simple analytical expression, whose predictions are shown to compare nicely with the microscopic cranking model calculations. For the $B_{\eta\eta}$ mass we get,

$$B_{\eta\eta} = \frac{AmR^2}{4}\left[\frac{v_t(1 + \gamma)}{v_c(1 + \delta^2)} - 1\right], \quad (11)$$

with

$$\gamma = \frac{R_c}{2R}\left[\frac{1}{1 + \cos\vartheta_1}\left(1 - \frac{R_c}{R_1}\right) + \frac{1}{1 + \cos\vartheta_2}\left(1 - \frac{R_c}{R_2}\right)\right], \quad (12)$$

$$\delta = \frac{1}{2R}[(1 - \cos\vartheta_1)(R_1 - R_c) + (1 - \cos\vartheta_2)(R_2 - R_c)], \quad (13)$$

$$v_c = \pi R_c^2 R, \quad (14)$$

and $v_t = v_1 + v_2$ is the total conserved volume. The ϑ_1 and ϑ_2 are the angles of the geometry of the model (see Fig. 1(b) of Ref. [41]). $R_c(\neq 0)$ is the radius of a cylinder of length R, having a homogeneous flow in it; whose existence is assumed for the mass transfer between the two spherical fragments. This formalism has been generalized for deformed nuclei by using the radii R_1 and R_2 for hot deformed nuclei, given by

$$R_i(\alpha_i, T) = R_{0i}(T)\left[1 + \sum_\lambda \beta_{\lambda_i} Y_\lambda^{(0)}(\alpha_i)\right], \quad (15)$$

where

$$R_{0i}(T) = \left[1.28A_i^{1/3} - 0.76 + 0.8A_i^{-1/3}\right](1 + 0.0007T^2), \quad (16)$$

and α_i represents the angle that the radius vector R_i of the colliding nuclei makes with the symmetry axis in clockwise direction.

The P_0 in Eq. (10) is given by the solution of stationary Schrödinger equation in η, at a fixed $R = R_a$,

$$\left\{-\frac{\hbar^2}{2\sqrt{B_{\eta\eta}}} \frac{\partial}{\partial\eta} \frac{1}{\sqrt{B_{\eta\eta}}} \frac{\partial}{\partial\eta} + V_R(\eta, T)\right\}\psi^\nu(\eta) = E^\nu\psi^\nu(\eta), \quad (17)$$

with $\nu = 0, 1, 2, 3...$, referring to ground-state ($\nu = 0$) and excited-state solutions summed over as a Boltzmann-like function

$$|\psi|^2 = \sum_{\nu=0}^\infty |\psi^\nu|^2 \exp(-E^\nu/T). \quad (18)$$

The temperature-dependent fragmentation potential $V_R(\eta, T)$ in Eq. (17) is the potential energy for all possible mass combinations A_i, corresponding to the given charges Z_i minimized for each mass fragmentation coordinate η and is defined as

$$
\begin{aligned}
V_R(\eta, T) = &\sum_{i=1}^{2} [V_{\text{LDM}}(A_i, Z_i, T)] + \sum_{i=1}^{2} [\delta U_i] exp\left(-\frac{T^2}{T_0^2}\right) \\
&+ V_c(R, Z_i, \beta_{\lambda_i}, \theta_i, T) + V_P(R, A_i, \beta_{\lambda_i}, \theta_i, T) \\
&+ V_\ell(R, A_i, \beta_{\lambda_i}, \theta_i, T),
\end{aligned} \tag{19}
$$

where V_p, V_c, V_l are temperature-dependent nuclear proximity, Coulomb, and angular momentum-dependent potentials, respectively, for deformed and oriented nuclei with deformation β_{λ_i}. The deformation parameters β_{λ_i} of the nuclei are taken from the tables of Möller *et al.* [42], and the orientations θ_i are the optimum [43] or compact orientations [44] of the "hot" process. $B_i = V_{\text{LDM}}(A_i, Z_i, T) + \delta U_i$ ($i = 1, 2$) are the temperature-dependent binding energies of two nuclei. $V_{\text{LDM}}(T)$ is the T-dependent liquid drop part of the binding energy by Davidson *et al.* [22] with modified pairing strength [45] and δU_i are the empirical shell corrections of Myers-Swiatecki [23]. $V_{\text{LDM}}(T)$ is taken from Davidson *et al.* [22], based on the semiempirical mass formula of Seeger [46], as

$$
\begin{aligned}
&V_{\text{LDM}}(A, Z, T) \\
&= \alpha(T)A + \beta(T)A^{2/3} + \left(\gamma(T) - \frac{\eta(T)}{A^{1/3}}\right)\left(\frac{I^2 + 2I}{A}\right) \\
&+ \frac{Z^2}{R_0(T)A^{1/3}}\left(1 - \frac{0.763}{Z^{2/3}} - \frac{2.29}{[R_0(T)A^{1/3}]^2}\right) \\
&+ \delta(T)\frac{f(Z, A)}{A^{3/4}},
\end{aligned} \tag{20}
$$

where

$$
I = a_a(Z - N), a_a = 1.0, \tag{21}
$$

and $f(Z, A) = (-1, 0, 1)$, for even-even, even-odd, and odd-odd nuclei, respectively. Temperature-dependent binding energies are obtained from Ref. [22] with its constants at $T = 0$ refitted [47,48] to give the ground state ($T = 0$) experimental binding energies [49], and, where the data is not available, the theoretical binding energies are taken from Ref. [42]. In the present work, we have inculcated the T-dependent RMF binding energies, with NL3 parameter set, by replacing the $V_{\text{LDM}}(A_i, Z_i, T) + \delta U_i$ terms of the fragmentation potential $V_R(\eta, T)$ defined in Eq. (19). The fragmentation potential $V_R(\eta, T)$ used in Eq. (17) embodies the nuclear structure effects and therefore, the preformation probability P_0 carriers the nuclear structure imprints.

For R coordinate motion, at a fixed η, the penetration probability is calculated by applying the WKB approximation as

$$
P = exp\left[-\frac{2}{\hbar}\int_{R_a}^{R_b}\{2\mu[V(R) - Q_{\text{eff}}]\}^{1/2}dR\right], \tag{22}
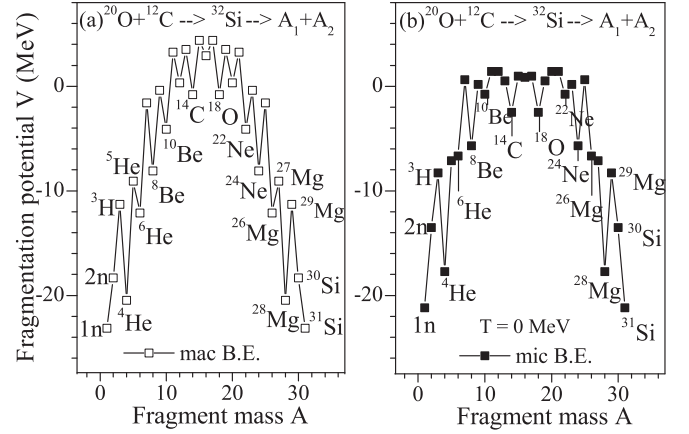$$

FIG. 1. Fragmentation potential V (MeV) in the decay of ^{32}Si at $T = 0$ MeV using (a) Davidson formula-based macroscopic (mac) B.E. and (b) RMF theory-based microscopic (mic) B.E.

where $V(R)$ is the scattering potential given by the addition of the last three terms in Eq. (19). It is solved analytically [50], with R_a as the first turning point.

The cross-section of CN decay termed as CN production cross section or fusion cross-section σ_{fus} is given as

$$
\sigma_{\text{fus}} = \sigma_{\text{LP}} + \sigma_{\text{IMF}} + \sigma_{\text{SMF}}, \tag{23}
$$

where σ_{LP}, σ_{IMF}, σ_{SMF} are the cross-section for light particles (LP), intermediate mass fragments (IMF), and symmetric mass fragments (SMF), respectively. The σ_{LP} consists of the contribution of neutron channels as well as light-charged particles (LCP). In the present work, the fusion cross-section associated with emission of LCP ($Z \leqslant 2$; $2 \leqslant A \leqslant 6$) is determined in reference to experimental measurements [9].

III. CALCULATIONS AND DISCUSSION

In this section, we discuss the dynamical aspects of ^{32}Si* nuclear system formed in ^{20}O + ^{12}C reaction and compare the DCM-calculated fusion cross-section with the experimental data. The fusion cross-section (σ_{fus}) is calculated via fragmentation potential, pre-existence/preformation probability of different fragments, and their subsequent penetration through scattering potential. The fragmentation potential consists of temperature-dependent Coulomb, proximity, and angular momentum-dependent potentials and temperature-dependent binding energies (T.B.E.) from Davidson mass formula with the addition of empirical shell corrections of Myers-Swaiticki. Here, we bring forth the significance of inculcation of RMF theory-based microscopic (mic) T.B.E. within DCM, to calculate the above-mentioned factors involved to evaluate the σ_{fus}, compared to the use of macroscopic (mac) T.B.E. from Davidson mass formula.

First, we investigate the fragmentation potential profile using mac and mic binding energies (B.E.) at $T = 0$ MeV comparatively, as presented in Fig. 1. Among light particles (LP), 1n, 2n, ^{3}H, and ^{4,5,6}He are noted in the fragmentation path. The structure of fragmentation potential and minimized/favored fragments essentially remains unchanged
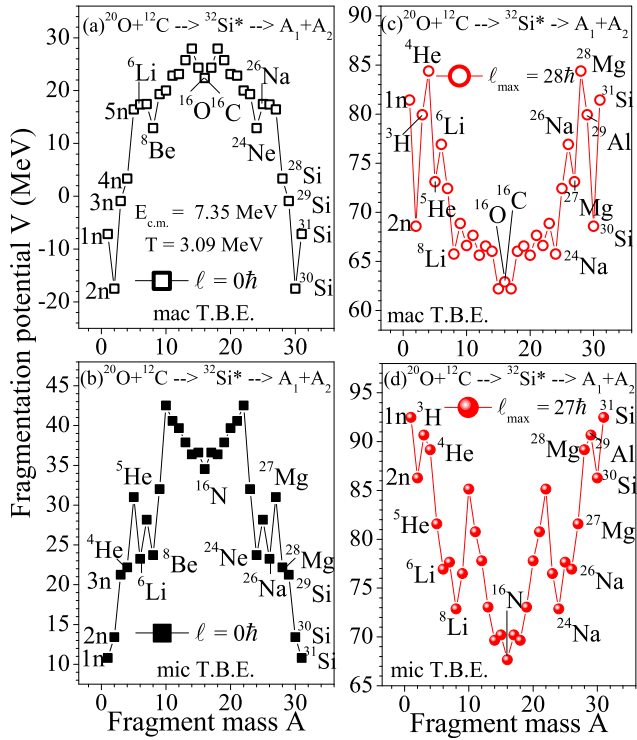
FIG. 2. Mass-dependence of fragmentation potential V (MeV) in the decay of ^{32}Si* formed at $T = 3.09$ MeV at $\ell = 0\,\hbar$ (left panel) and ℓ_{max} value (right panel) using (a, c) Davidson formula-based macroscopic T.B.E. and (b, d) RMF theory-based microscopic T.B.E.
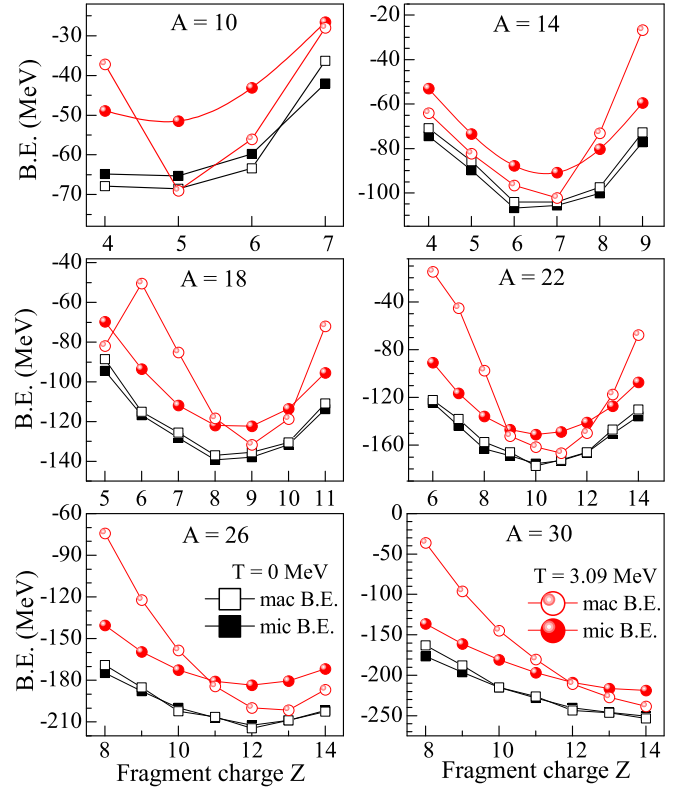

FIG. 3. The macroscopic and microscopic binding energies (B.E.) for some isobars with mass number $A = 10, 14, 18, 22, 26, 30$ at $T = 0$ MeV and 3.09 MeV obtained using Davidson formula and RMF theory, respectively.

with a small change in the magnitude for mac and mic B.E. cases. It is due to the fact that both mac and mic B.E. using Davidson mass formula and RMF theory, respectively, are nearly similar and well compared with the experimental binding energy data at $T = 0$ MeV. However, the difference in B.E. at higher temperature is anticipated depending upon the method (mass formula or theory) involved to calculate the T.B.E. To elucidate the impact of mac and mic T.B.E., calculated from Davidson formula and RMF theory comparatively, upon the fragmentation process the fragmentation potential [Eq. (19)] of ^{32}Si* nuclear system is shown in Fig. 2. The left panel [Figs. 2(a) and 2(b)] presents the fragmentation potential at $\ell = 0\,\hbar$ and right panel [Figs. 2(c) and 2(d)] presents the fragmentation potential at $\ell = \ell_{max}$ for mac and mic T.B.E. cases. At a lower ℓ-value, it is clear that LP or equivalently evaporation residues (ER) are favored energetically for both the cases of T.B.E. [Figs. 2(a) and 2(b)]. For the mac T.B.E. case, the neutrons (1n-5n) are the most probable exit channels in the decay process [Fig. 2(a)]. However, for mic T.B.E. case, in addition to neutron channels, the α channels (^{4}He, ^{5}He) with complementary ^{28}Mg, ^{27}Mg (or xn-$x\alpha$, x is an integer) channels also come into the picture [Fig. 2(b)]. This observation is in accordance with predictions of the statistical EVAPOR model [9] giving ^{5}He as one of the probable light particle emission channels. Other α-like fragments (^{8}Be, ^{24}Ne) are also more favored energetically for mic T.B.E. compared to mac T.B.E. case. It is also noted that a higher value of fragmentation potential for LP (or ER) for

the mic T.B.E. case than the mac T.B.E. dictates that ^{32}Si* becomes more prone/unstable with respect to the emission of LP. The structure of symmetric mass fragments (SMF) also gets changed with the inculcation of mic T.B.E.

At ℓ_{max}-value, among LP, in addition to neutron channels, the tritium, α, and ^{5}He exit channels with complementary ^{29}Al, ^{28}Mg, and ^{27}Mg, respectively, are seen due to change in Z-distribution for mac T.B.E. [Fig. 2(c)]. Whereas, the ^{4}He, ^{5}He seen at ℓ_{max}-value are also preformed at lower ℓ-value for mic T.B.E. case. At ℓ_{max}-value, the symmetric mass fragments (SMF) are energetically minimized compared to LP. The intermediate mass fragments (IMF) are also in competition with SMF. Quite interestingly, the shape of the potential energy surface changes significantly for light particles and SMF window ($A_{CN}/2\pm5$) for mic T.B.E. case.

It is inferred from Fig. 2 that structure and magnitude of fragmentation potential change significantly along with some changes in Z-distribution by taking into account the mic T.B.E. In other words, T.B.E. governs the shape of the potential energy surface. The mic B.E., calculated within RMF theory, of some isobars with $A = 10, 14, 18, 22, 26,$ and 30 at $T = 0$ MeV and 3.09 MeV are shown along with Davidson mass formula-based mac B.E. in Fig. 3. At $T = 0$ MeV, there is a negligible difference in the magnitude of mac and mic B.E. However at higher temperature $T = 3.09$ MeV, the magnitude as well as the shape of binding energy parabola is quite different for theory and mass formula computed
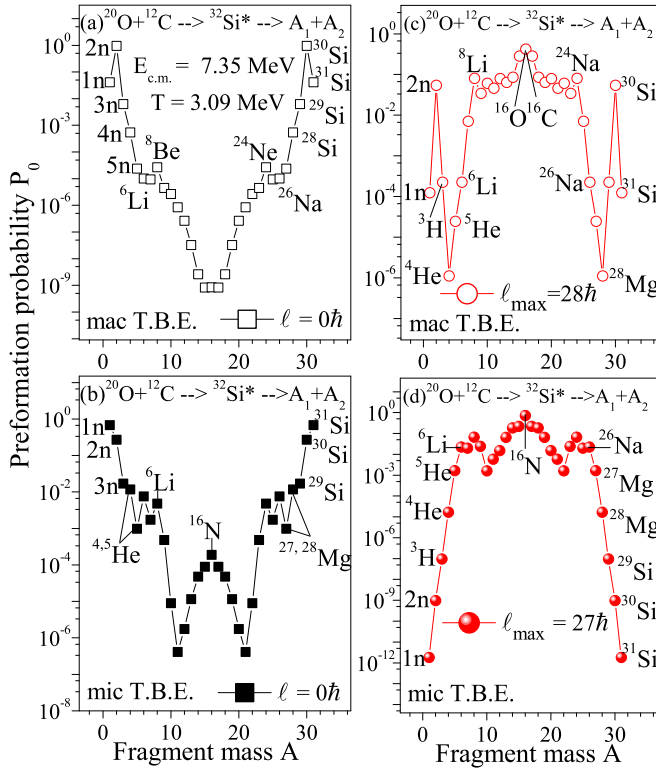
FIG. 4. Preformation probability P_0 of different fragments in the decay of ^{32}Si* formed at $T = 3.09$ MeV at $\ell = 0$ $\hbar$ (left panel) and ℓ_{max} value (right panel) using (a, c) Davidson formula-based macroscopic T.B.E. and (b, d) RMF theory-based microscopic T.B.E.

FIG. 5. Same as Fig. 4 but for replaced light-charged particles (LCP).

T.B.E. The mic T.B.E. vary smoothly compared to mac T.B.E. at $T = 3.09$ MeV for all shown isobars. It is important to mention here that the Davidson formula-based mac B.E. are calculated via empirical fitting of constants in reference to available experimental data at $T = 0$ MeV. But the divergence of results using mass formulas in unknown regions with no common trend is noted by considering one of the available mass reference cases, which raises the question about their predictive power [25,26], as also discussed in the introduction part. However, RMF theory-based mic B.E. are fitted for only a few doubly magic nuclei in reference to experimental data at $T = 0$ MeV and predictions made for thousands of nuclei agree with experimental data. It portrays the intrinsic predictive efficacy of RMF theory and therefore RMF theory-based mic T.B.E. are much reliable.

Further, we will explore the nuclear structure effects in the decay of ^{32}Si* via preformation probability P_0 calculations within the collective clusterization approach of DCM. The fragmentation potential being an essential input in the preformation probability calculations [see Eq. (17)] encompass the nuclear structure imprints in the preformation probability P_0 of different fragments. The energetically minimized fragments in the fragmentation profile are stable and therefore will be highly preformed. Figure 4 presents the preformation probability of different fragments for two different choices of T.B.E. at $T = 3.09$ MeV. The preformation profile evolves from an asymmetric [Figs. 4(a) and 4(b)] to a symmetric [Figs. 4(c) and 4(d)] one while moving from lower to higher
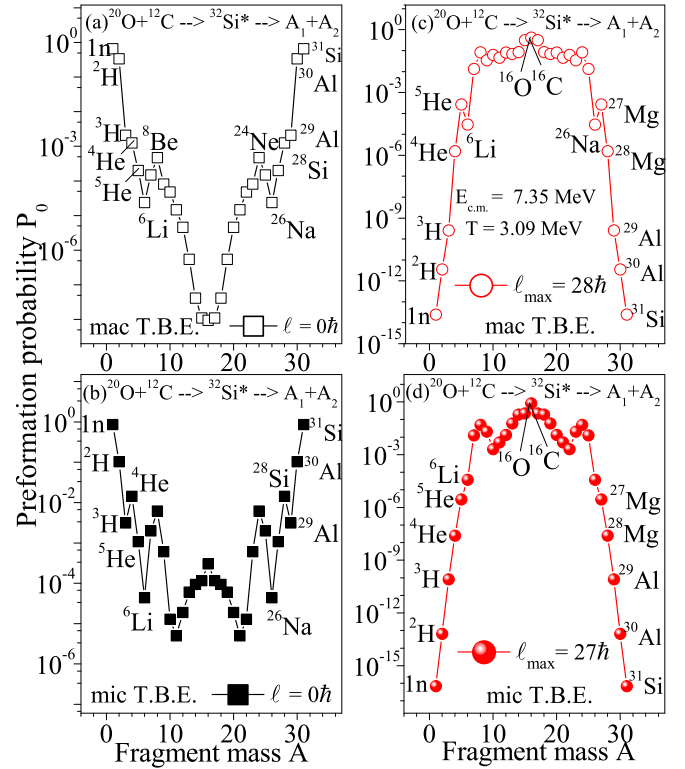
ℓ-value for both cases of T.B.E. At $\ell = 0\hbar$, neutrons are the most probable LP channels for mac T.B.E. [Fig. 4(a)], whereas α channels (^{4}He, ^{5}He) with complimentary xn-$x\alpha$ channels (^{28}Mg, ^{27}Mg) are also preformed among LP for mic T.B.E. case [Fig. 4(b)], as discussed earlier. It is noted that P_0 of 2n is more than 1n for mac T.B.E. whereas the 1n is having highest P_0 value for mic T.B.E. At $\ell = \ell_{max}$, SMF are highly preformed and IMF are also competing with SMF. Among LP, 2n channel competes with IMF and SMF even at higher ℓ-value for mac T.B.E. case [Fig. 4(c)]. The P_0 value of α channels (^{4}He, ^{5}He) is more for mic T.B.E. case [Fig. 4(d)] compared to mac T.B.E case [Fig. 4(c)]. The shape of preformation profile changes notably for light particles and SMF window by consideration of mic T.B.E [Fig. 4(d)].

The nuclear system ^{32}Si* undergo de-excitation via emission of neutron, proton, and α particles resulting in ER. Although, the major fraction of ER is formed via the neutron emission channels but a significant proportion of ER is formed via emission of LCPs. It is important to note that experimentally measured fusion cross-section involve contributions of LCP ($Z \leqslant 2$, $2 \leqslant A \leqslant 6$) only [9], therefore fusion cross-section is evaluated by the addition of contribution of each LCP channel. To calculate fusion cross-section of LCP (σ_{fus}), we have chosen in the fragmentation potential profile the ^{2}H, ^{3}H, ^{4}He, ^{5}He, ^{6}He LCP in place of 2n, 3n, 4n, 5n, ^{6}Li for mac T.B.E. case and ^{2}H, ^{3}H, and ^{6}He LCP instead of 2n, 3n, and ^{6}Li for mic T.B.E. case. The preformation profile for mac and mic T.B.E. cases at T = 3.09 MeV with replaced LCP is shown in Fig. 5.
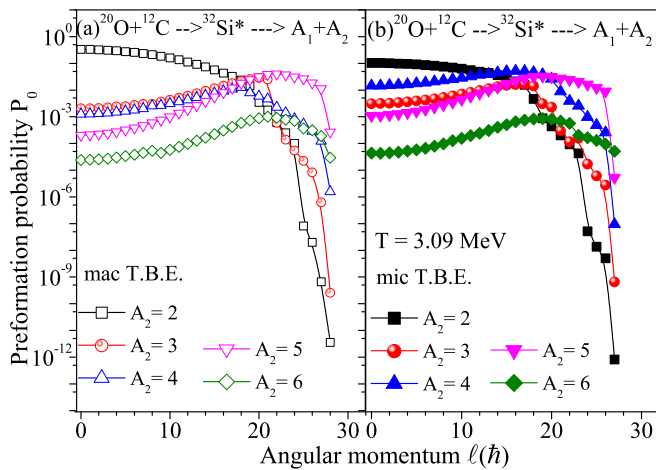
FIG. 6. Angular momentum dependence of preformation probability P_0 of LCP for ^{32}Si* nuclear system formed at $T = 3.09$ MeV for (a) mac T.B.E. and (b) mic T.B.E. case.

The variation of P_0 with angular momentum for chosen LCP channels is shown in Fig. 6 for both T.B.E. cases. For ^{2}H, the P_0 decreases with an increase in ℓ-value, while for other LCP channels the P_0 rises up to $\ell = 18$–20 $\hbar$ and decreases afterward for both T.B.E. cases. For mic T.B.E. case, the P_0 of ^{4}He is more than ^{3}H compared to mac T.B.E. case. ^{5}He LCP channel has also a higher value of P_0 for mic T.B.E. than in mac T.B.E. case. Another important factor in the fusion cross-section calculations is the penetrability of LCP through scattering potential. Figure 7 presents the scattering potential for ^{3}H, ^{4}He, ^{5}He with ^{29}Al, ^{28}Mg, ^{27}Mg complimentary
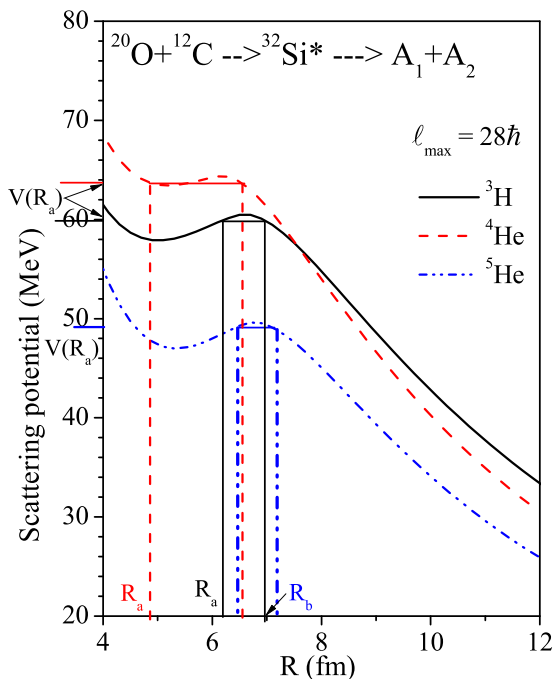

FIG. 7. Scattering potential for the emission of ^{3}H, ^{4}He, ^{5}He with complimentary ^{29}Al, ^{28}Mg, ^{27}Mg channels, respectively, in the decay of ^{32}Si* nuclear system at $T = 3.09$ MeV.
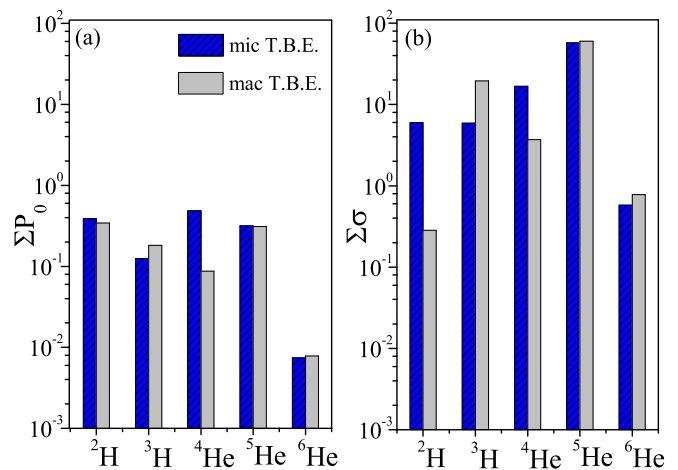

FIG. 8. (a) Summed up preformation probability ΣP_0 and (b) summed up cross-section $\Sigma \sigma$ of different LCP channels in the decay of ^{32}Si* nuclear system formed at T = 3.09 using mac and mic T.B.E.

channels, respectively, at ℓ_{max} value. R_a and R_b present the first and second turning points. It is noted that the barrier is lowest for ^{5}He compared to ^{3}H, ^{4}He channels. It may be due to the centrifugal effect, since the angular momentum-dependent potential is high for lighter ^{3}H and ^{4}He channels. Among ^{4}He and ^{5}He channels, the Coulomb barrier is reduced for n-rich ^{5}He.

It is noted that we have performed calculations using the collective clusterization approach of the DCM, which means that the relative contribution of all possible binary fragments in the decay channel is accounted via preformation probability (P_0). Here, the relative fragmentation is analyzed in terms of preformation probability, which encompasses the structure effects at the compound nucleus level. The barrier penetration, however, contributes only toward the magnitude of the cross-section. Therefore, one-dimensional WKB approximation is employed to estimate penetrability. It is relevant to note that WKB penetrability gives a reasonable account of the tunneling process, as evident from Ref. [51].

Further, the effect of change in the structure of fragmentation/preformation profile, with the inclusion of microscopic T.B.E., upon fusion cross-section calculations is speculated. Figure 8(a) presents the summed up preformation probability ΣP_0 of LCP. The ΣP_0 of ^{4}He is considerably larger in case of mic T.B.E. compared to mac T.B.E. case, whereas for ^{5}He and ^{6}He the value of ΣP_0 is approximately the same for both cases of T.B.E. These preformed LCP contributes toward cross-section and their summed up cross-section $\Sigma \sigma$ is shown in Fig. 8(b) for mic and mac T.B.E cases. It is noted that ^{5}He is the major contributor in σ_{fus} for both mac and mic T.B.E. cases. It is probably due to the low barrier for ^{5}He leading to higher penetrability through the interaction barrier (Fig. 7) although its preformation probability P_0 is less compared to other LCP channels. This result is in line with statistical EVAPOR model calculations [9] depicting the more percentage contribution of ^{5}He channels among different LCP channels. For mic T.B.E case, the contribution of ^{2}H and ^{4}He channels is relatively enhanced while that of ^{3}H channel is

TABLE I. The fusion cross-section associated with light-charged particles (LCP) in ^{20}O + ^{12}C reaction calculated within DCM using macroscopic (mac) and microscopic (mic) T-dependent binding energies (T.B.E.) from Davidson formula and using RMF theory, respectively, along with a comparison with other model results and experimental data [9].

$E_{c.m.}$ (MeV)	T (MeV)	ℓ_{max} ($\hbar$)	mac T.B.E. $\sigma(A_i)$ (mb)	σ_{fus}^{DCM} (mb)	ℓ_{max} ($\hbar$)	mic T.B.E. $\sigma(A_i)$ (mb)	σ_{fus}^{DCM} (mb)	σ_{fus}^{Bass} (mb)	σ_{fus}^{TDHF} (mb)	σ_{fus}^{Expt} (mb)
7.35	3.09	28	$\sigma_{2H} = 0.28$ $\sigma_{3H} = 19.48$ $\sigma_{4He} = 3.70$ $\sigma_{5He} = 60.0$ $\sigma_{6He} = 0.78$	84.2	27	$\sigma_{2H} = 5.96$ $\sigma_{3H} = 5.87$ $\sigma_{4He} = 16.72$ $\sigma_{5He} = 57.35$ $\sigma_{6He} = 0.58$	86.5	1.8	24.2	82.3 ± 26
9.29	3.18	28	$\sigma_{2H} = 0.30$ $\sigma_{3H} = 39.56$ $\sigma_{4He} = 4.20$ $\sigma_{5He} = 82.31$ $\sigma_{6He} = 0.82$	127.6	27	$\sigma_{2H} = 1.96$ $\sigma_{3H} = 12.88$ $\sigma_{4He} = 26.81$ $\sigma_{5He} = 77.31$ $\sigma_{6He} = 0.96$	119.6	59	92.2	133.4 ± 37

low compared to the case of mac T.B.E. The values of ΣP (not shown here) are nearly similar for both cases of T.B.E. for each LCP channel. Therefore, it is evident that the trend in $\Sigma\sigma$ is due to ΣP_0 signifying that nuclear structure information is carried by P_0 and the cross-sections follow the trend of P_0 for mic and mac T.B.E. choices. These results are also shown in Table I, which presents the DCM-calculated fusion cross-section associated with LCP (σ_{fus}^{DCM}) using mac and mic T.B.E. from Davidson formula and using RMF theory, respectively. With an increase in $E_{c.m.}$, the σ_{fus} associated with LCP emission increases. At higher $E_{c.m.}$, the contribution of the ^{2}H channel decreases than at $E_{c.m.} = 7.35$ MeV while the contribution of the ^{3}H channel increases at higher $E_{c.m.}$, in accordance with statistical EVAPOR model results [9]. The inculcation of mic T.B.E. within DCM shows a significant contribution of the α particle (^{4}He) in the σ_{fus} associated with LCP at both energies. The results of the standard fusion Bass model and DC-TDHF model are also shown, which underpredict the σ_{fus} at both energies. Whereas the experimentally measured σ_{fus} for neutron-rich ^{20}O + ^{12}C system is reproduced well within the collective clusterization approach of DCM.

IV. SUMMARY

We have investigated the reaction involving neutron-rich ^{20}O nucleus, which is of considerable importance in the astrophysical environment. The role of microscopic (mic) temperature-dependent binding energies (T.B.E.) upon the different factors involved in the fusion cross-section calculations of neutron-rich ^{20}O + ^{12}C system has been explored within the quantum mechanical fragmentation theory-based dynamical cluster-decay model (DCM). The fragmentation potential, used to estimate the nuclear structure effects via preformation probability of different fragments, involves temperature-dependent nuclear, Coulomb, centrifugal potentials together with T.B.E. With the inculcation of RMF theory-based mic T.B.E, a considerable change in the minimized/favored fragments and structure of fragmentation potential is noted compared to macroscopic (mac) T.B.E. calculated using Davidson mass formula. The α and α-like fragment (^{5}He) are favored energetically at all ℓ-values for the mic T.B.E. case in line with statistical EVAPOR model results whereas only neutrons are preformed at lower ℓ-values for mac T.B.E case. Subsequently, it affects the preformation profile of different fragments and the contribution of individual LCP channels in the fusion cross-section (σ_{fus}). The inculcation of mic T.B.E. predict/give a significant contribution of the α particle (^{4}He) in σ_{fus} associated with LCP and ^{5}He is the dominant LCP channel contributing in σ_{fus}. The Bass model and DC-TDHF model underpredict the fusion cross-section associated with LCP emission whereas DCM-calculated σ_{fus} are in good agreement with the available experimental data.

[1] P. F. F. Carnelli, S. A. Calderon, K. E. Rehm, M. Albers *et al.*, Phys. Rev. Lett. **112**, 192701 (2014).

[2] J. F. Liang, C. J. Gross, Z. Kohley, D. Shapira *et al.*, Phys. Rev. C **85**, 031601(R) (2012).

[3] J. F. Liang, D. Shapira, C. J. Gross, J. R. Beene *et al.*, Phys. Rev. Lett. **91**, 152701 (2003).

[4] A. S. Umar, V. E. Oberacker, and C. J. Horowitz, Phys. Rev. C **85**, 055801 (2012).

[5] C. J. Horowitz and D. K. Berry, Phys. Rev. C **79**, 065803 (2009).

[6] C. J. Horowitz, H. Dussan, and D. K. Berry, Phys. Rev. C **77**, 045807 (2008).

[7] W. Loveland, A. M. Vinodkumar, R. S. Naik, P. H. Sprunger *et al.*, Phys. Rev. C **74**, 064609 (2006).

[8] A. M. Stefanini, L. Corradi, A. M. Vinodkumar, Y. Feng *et al.*, Phys. Rev. C **62**, 014601 (2000).

[9] M. J. Rudolph, Z. Q. Gosser, K. Brown, S. Hudan *et al.*, Phys. Rev. C **85**, 024605 (2012).

[10] R. Bass, Phys. Rev. Lett. **39**, 265 (1977).

[11] K. Godbey, A. S. Umar, and C. Simenel, Phys. Rev. C **95**, 011601(R) (2017).

[12] A. A. V. Karpov, V. A. Rachkov, and V. V. Samarin, Phys. Rev. C **92**, 064603 (2015).

[13] V. N. Kondratyev, A. Bonasera, and A. Iwamoto, Phys. Rev. C **61**, 044613 (2000).

[14] R. K. Gupta, *Lecture Notes in Physics*, edited by C. Beck, Lecture Notes in Physics 818, Vol. I (Springer Verlag, 2010), p. 223.

[15] M. Kaur, B. B. Singh, S. K. Patra, and R. K. Gupta, Phys. Rev. C **95**, 014611 (2017); M. Kaur, B. B. Singh, and S. K. Patra, Indian J. Pure App. Phys. **57**, 584 (2019).

[16] M. Kaur, B. B. Singh, S. Kaur, and R. K. Gupta, Phys. Rev. C **99**, 014614 (2019).

[17] B. B. Singh and M. Kaur, *Nuclear Structure Physics*, edited by A. Shukla and S. K. Patra (Taylor & Francis Group, 2020), pp. 145–166.

[18] M. Kaur, B. B. Singh, M. K. Sharma, and R. K. Gupta, Nucl. Phys. A **969**, 14 (2018).

[19] R. Kaur, M. Kaur, V. Singh, S. Kaur, B. B. Singh, and B. S. Sandhu, Phys. Rev. C **98**, 064612 (2018).

[20] R. Kaur, S. Kaur, B. B. Singh, B. S. Sandhu, and S. K. Patra, Phys. Rev. C **101**, 034614 (2020).

[21] V. M. Strutinsky, Nucl. Phys. A **95**, 420 (1967).

[22] N. J. Davidson, S. S. Hsiao, J. Markram, H. G. Miller, and Y. Tzeng, Nucl. Phys. A **570**, 61 (1994).

[23] W. D. Myers and W. D. Swiatecki, Nucl. Phys. A **81**, 1 (1966).

[24] W. Mittig, P. Roussel-Chomaz, and A. C. C. Villari, *Europhysics News* Vol. 35, No. 4 (2004), https://www.europhysicsnews.org/articles/epn/abs/2004/04/contents/contents.html.

[25] S. K. Patra, P. Arumugam, and L. Satpathy, arXiv:nucl-th/0504063.

[26] R. C. Nayak and L. Satpathy, Atomic Data and Nucl. Data Tables **98**, 616 (2012).

[27] A. Quddus, K. C. Naik, and S. K. Patra, J. Phys. G: Nucl. Part. Phys. **45**, 075102 (2018).

[28] M. Kaur, A. Quddus, A. Kumar, M. Bhuyan, and S. K. Patra, Nucl. Phys. A **1000**, 121871 (2020).

[29] M. Kaur, A. Quddus, A. Kumar, and S. K. Patra, J. Phys. G: Nucl. Part. Phys. **47**, 105102 (2020).

[30] R. J. Furnstahl, B. D. Serot, and H. B. Tang, Nucl. Phys. A **598**, 539 (1996); **615**, 441 (1997).

[31] M. Del Estal, M. Centelles, X. Viñas, and S. K. Patra, Phys. Rev. C **63**, 044321 (2001); **63**, 024314 (2001).

[32] P. G. Blunden and M. J. Iqbal, Phys. Lett. B **196**, 295 (1987).

[33] P. G. Reinhard, Rep. Prog. Phys. **52**, 439 (1989).

[34] J. W. Negele, Phys. Rev. C **1**, 1260 (1970).

[35] D. G. Madland and J. R. Nix, Nucl. Phys. A **476**, 1 (1988).

[36] S. K. Patra, Phys. Rev. C **48**, 1449 (1993).

[37] Y. K. Gambhir, P. Ring, and A. Thimet, Ann. Phys. **198**, 132 (1990).

[38] J. Marhun and W. Greiner, Phys. Rev. Lett. **32**, 548 (1974).

[39] H. J. Fink, J. Marhun, W. Scheid, and W. Greiner, Z. Phys. **268**, 321 (1974).

[40] R. K. Gupta, W. Scheid, and W. Greiner, Phys. Rev. Lett. **35**, 353 (1975).

[41] H. Kröger and W. Scheid, J. Phys. G **6**, L85 (1980).

[42] P. Möller, J. R. Nix, W. D. Myers, and W. J. Swiatecki, At. Data Nucl. Data Tables **59**, 185 (1995).

[43] R. K. Gupta, M. Balasubramaniam, R. Kumar, N. Singh, M. Manhas *et al.*, J. Phys. G **31**, 631 (2005).

[44] R. K. Gupta, M. Manhas, and W. Greiner, Phys. Rev. C **73**, 054307 (2006).

[45] M. Bansal, R. Kumar, and R. K. Gupta, J. Phys. Conf. Series **321**, 012046 (2011).

[46] P. A. Seeger, Nucl. Phys. **25**, 1 (1961).

[47] R. K. Gupta, R. Kumar, N. K. Dhiman, M. Balasubramaniam, W. Scheid, and C. Beck, Phys. Rev. C **68**, 014610 (2003).

[48] B. B. Singh, M. K. Sharma, and R. K. Gupta, Phys. Rev. C **77**, 054613 (2008).

[49] G. Audi and A. H. Wapstra, Nucl. Phys. A **595**, 409 (1995); G. Audi, A. H. Wapstra, and C. Thiboult, *ibid.* **729**, 337 (2003).

[50] S. S. Malik and R. K. Gupta, Phys. Rev. C **39**, 1992 (1989).

[51] D. Jain *et al.*, Eur. Phys. J. A **50**, 155 (2014).